RSC Advances

PAPER

View Article Online
View Journal | View Issue

Cite this: *RSC Adv.*, 2020, **10**, 29336

Assessment of *in vitro* cytotoxicity of imidazole ionic liquids and inclusion in targeted drug carriers containing violacein†

Ignacio Rivero Berti,[a] Boris Rodenak-Kladniew,[b] Celeste Onaindia,[c] Claudia G. Adam,[c] German A. Islan,[a] Nelson Durán[de] and Guillermo R. Castro[a]

Received 9th June 2020
Accepted 17th July 2020

DOI: 10.1039/d0ra05101b

rsc.li/rsc-advances

Violacein (Viol) is a pigment produced by several Gram-negative bacteria with many bioactivities, such as anticancer, virucide, and antiparasitic. However, violacein is insoluble under physiological conditions preventing its potential therapeutic uses. Surface-active ionic liquids (SAILs) based on the cation 1-alkylimidazolium ([C_nHim]) with n = 10 to 16 alkyl carbon side chain lengths and acetate, bromide, methanesulfonate (S) or trifluoroacetate (F) as counterions were synthesized and screened to dissolve Viol in micellar aqueous media and for toxicological studies on the human lung carcinoma A549 cell line. Screening allowed the selection of 1.5 × 10^{-3}% (w/v) [C_{16}Him]-S because it combines low cytotoxicity with 71.5% cell viability and good interaction with 95.2% of the violacein kept in micellar solution for at least 48 h. [Viol-([C_{16}Him]-S)] complex was used to develop an efficient hybrid solid lipid nanoparticle (SLN) carrier based on myristyl myristate and poloxamer 188 and tailored with folate to target cancer cells. Cellular SLN uptake was evaluated with fluorescent $DiOC_{18}$ on A549, HCT-116, and HeLa cell lines expressing or not the folate receptor. The results showed fivefold incorporation of Viol nanoparticles in HCT-116 and HeLa cell cultures, displaying a high level of folate receptor. Biophysical characterization of the hybrid solid lipid carrier containing Viol was performed by dynamic light scattering, Fourier transform infrared, X-ray diffraction and X-ray photoelectron spectroscopies, and by transmission electron and cryo-transmission microscopies.

Introduction

Violacein (Viol) is a purple bisindole bacterial pigment synthesized in the presence of two precursor tryptophan molecules through six enzymatic steps and produced by diverse genera of Gram-negative bacteria. Viol is released from bacteria *via* membrane vesicles.[1]

Several potential clinical uses of Viol are described in the literature such as microbiocide activity targeting the cytoplasmic membrane of Gram-positive microorganisms,[2,3] antiplasmodial and trypanocidal,[4] analgesic,[5] antitumoral and virucide among others recently reviewed.[6] Additionally, Viol was reported as an immunostimulatory molecule that is mediated by TLR8 and relevant for immunosuppressed patients.[7]

Cancer is the second leading cause of death in the world reported by WHO, accounting for 18 million new diagnosed cases and 9.5 million deaths regardless of gender and age in 2018.[8] Particularly, the need for new treatments and novel drug alternatives arises, and the role of Viol as potential antitumoral agent is of great interest. Viol has been tested in several tumour cell lines such as HL60 leukaemia,[9] MCF7 breast cancer,[10] U87 glioblastoma, A549 lung cancer,[11] and HT29, Caco-2 and HCT116 colorectal cancer lines,[12–14] among many others, with positive results. The antitumor activity of Viol in chemoresistant human leukaemia cells was investigated and involves several mechanisms such as activation of protein kinases (*i.e.* PKA, AKT, and PDK) but also inhibition of calpain and death-associated protein kinase 1 (APK1) leading to kinome reprogramming, stress of endoplasmic reticulum, Golgi apparatus failure with consequent cell death.[15] Also, *in vivo* Viol antitumoral activity was previously confirmed and reported elsewhere.[13,16]

However, the bisindole structure of Viol makes it practically insoluble in aqueous solutions, similarly to many molecules with anticancer activity. Aromatic–aromatic interactions

[a]*Laboratorio de Nanobiomateriales, CINDEFI, Departamento de Química, Facultad de Ciencias Exactas, Universidad Nacional de La Plata-CONICET (CCT La Plata), Calle 47 y 115, B1900AJL La Plata, Argentina. E-mail: grcastro@gmail.com*

[b]*Instituto de Investigaciones Bioquímicas de La Plata (INIBIOLP), CONICET-UNLP, CCT-La Plata, Facultad de Ciencias Médicas, B1900 La Plata, Argentina*

[c]*IQAL, Instituto de Química del Litoral (UNL-CONICET), Facultad de Ingeniería Química-Universidad Nacional del Litoral, Santiago del Estero 2829, Santa Fe, 3000, Argentina*

[d]*Institute of Biology, Universidade Estadual de Campinas, C.P. 6159, CEP 13083-970, Campinas, SP, Brazil*

[e]*NanoMed Center, Federal University of ABC (UFABC), Santo André, SP, Brazil*

† Electronic supplementary information (ESI) available. See DOI: 10.1039/d0ra05101b

through hydrophobic motifs are commonly described as a competition between stacking, T-shaped or crossed complexes, which is determined by the characteristics of the environment and the chance of hydrogen bond formation between polar residues and the solvent. In the case of Viol, the presence of indole chemical structure could form T-shaped complexes as was similarly described for tryptophan–tryptophan interactions, which is the precursor molecule of the pigment.[17,18] In addition, the formation of T-shaped Viol complexes could be responsible for some toxicity to normal cells since the pigment shows very limited solubility in physiological environments. Consequently, the potential use of Viol as a drug of pharmaceutical interest depends on the development of novel formulations that improve solubility and bioavailability concomitantly with the reduction of adverse effects on healthy tissues.

Ionic liquids (ILs) are organic salts with melting points typically below 100 °C. ILs possess a wide range of properties such as low vapor pressure, dissolution capabilities, and good thermal stability.[19] Different combinations of cations, anions, and substituents can produce a myriad of different ILs and therefore, it is possible to tailor and tune their physicochemical properties such as solvation, viscosity, hydrophobicity, surfactant properties, ionic interactions, and biological aspects such as cytotoxicity and biodegradability.[19] Because of these interesting properties, many ILs have been synthesized in the last decades and are considered as green solvents for extraction and chemical synthesis, biocatalysis and biotechnology applications.[20] In a recent work, a new series of SAILs based on the cation 1-alkylimidazolium **[C$_n$Him]** (with alkyl chain length from 7 to 16) containing methanesulfonate ([$CH_3SO_3^-$], S) and trifluoroacetate ([$CF_3CO_2^-$], F) as counterion was presented. Their self-aggregation properties in aqueous solutions were studied. These SAILs display spontaneous self-assembly properties and a range of critical micellar concentrations (CMC) from 104.3 mM to 0.4 mM depending on the cation–anion relationship. It was reported that the increase of alkyl carbon length in the cation from 7 to 16 reduced the CMC about 100 and 150 times for both counterions analysed.[21] These new types of ILs with surfactant properties could allow tailoring the interaction with different molecules "on demand". Particularly, the SAIL of type **[C$_n$Him]**-S or **[C$_n$Him]**-F could help develop drug delivery devices of hydrophobic molecules since many drugs cannot reach the pharmaceutical market because of low solubility issues.

However, one of the main concerns for the use of ILs in the biofield (*e.g.* biomedicine, medicine, pharmaceuticals) is related to the toxicity to mammalian cells because of the lack of rational and systematic studies. The main approach to reduce and/or avoid toxic effects is to use biocompatible cations and anions. Recent studies of ILs in the pharmaceutical field focus on the search and development of three main applications such as drug delivery, surfactants or co-solvents, and active pharmaceutical ingredients.[22] Particularly, the use of ILs in drug delivery has attracted great attention because approximately 90% of the drugs in the market showed poor solubility in aqueous media.[23] Since 2012, many drug and prodrug formulations made using ILs have been reported. Examples of recently reviewed drugs formulated on different ILs are albendazole, acyclovir, cinnamic acid, danazol, ibuprofen, lidocaine, methotrexate, penicillin, piperacillin, piroxicam, and sulfacetamide.[22,24]

Nanotechnology for the development of drug delivery systems is known to overcome solubility and bioavailability issues. First, since the drug can be dispersed in the matrix at nanometric scale, the solubility of the drug is no longer a limit for its therapeutic use. On the other hand, nanocarriers can provide controlled and localized release kinetics of the active drug by passive (*i.e.* enhanced permeability and retention) or active (by coating the carrier with ligands for specific receptors) targeting.[25] For example, folate or ferritin are commonly reported to provide active targeting by decorating particle surfaces. Particularly, folate is a highly reported targeting agent for cancer treatment, as folate receptors are overexpressed in some cancer cells (*i.e.* HCT-116 and HeLa) and possess low or undetectable levels of expression in normal cells and some cancer cells (*i.e.* A549 cell line). The folate receptor is broadly distributed in tumor cells, while its expression is very limited in normal tissues and organs.[26] For example, folate receptors displayed high expression typically in brain, breast, cervical, colorectal, epithelial, kidney, lung, and ovarian tumors. Folate receptors also have the advantage of promoting endocytosis and consequently, internalization of nanoparticles.[27] Among, nanodrug delivery systems, solid lipid nanoparticles (SLN) are drug carriers developed in the 1990s and used for encapsulation of many drug models. Generally, SLNs possess high encapsulation efficiency in poor water-soluble drugs, high stability, and are biocompatible and biodegradable. Also, among the main advantages of SLNs are the possibility of combining diverse lipids with different physicochemical properties and being able to form solid lipid hybrid structures named nanostructured lipid carriers (NLC), which are easy to scale up.[25] Another advantage of SLNs for the treatment of cancer is the highly acid cytosolic environment that allows hydrolysing the lipid esters and consequently disassembling the nanoparticle structure and therefore, releasing the drug inside the cell.

In the present work, cytotoxicity screening of **[C$_n$Him]**-S and **[C$_n$Him]**-F with n from 10 to 16 carbon side chain length on human lung carcinoma A549 was performed to determine the relationship between chemical structure and toxicity. Also, to deepen the analysis and compare behaviours, [C_{16}Him] with acetate $(CH_3CO_2)^-$ as counterion and 1-hexadecyl-3-methylimidazolium ([C_{16}mim]) with bromide $(Br)^-$ as counterion were also synthesized. Viol as anticancer drug model was produced, purified, and characterized by spectroscopic methods. Additionally, the interaction of the SAILs, **[C$_n$Him]**-S and **[C$_n$Him]**-F with Viol was analyzed. NLCs containing myristyl myristate and poloxamer P188 or ILs were produced, followed by surface modification with folate for cell targeting. Physicochemical characterization of the selected systems by dynamic light scattering, Fourier transform infrared (FTIR), X-ray photoelectron (XPS) and X-ray diffraction (XRD) spectroscopies, also by transmission electron microscopy (TEM) and CryoTEM was performed. Cytotoxicity tests (MTT) of ILs on

adenocarcinoma human alveolar basal epithelial A549 cell line and of NLC on HeLa cervical cancer, HCT116 metastatic colorectal adenocarcinoma, and A549 cell lines were conducted. Finally, studies on cell uptake of the selected Viol-SLN-IL formulation containing folic acid in the three cell lines were performed using $DiOC_{18}$ green fluorescent tracer and evaluated by fluorescent microscopy.

Experimental

Reagents

Violacein [3-(1,2-dihydro-5-(5-hydroxy-1*H*-indol-3-yl)-2-oxo-3*H*-pyrrol-3-ylidene)-1,3-dihydro-2*H*-indole-2-one] was produced from Chromobacterium violaceum following previous protocols published elsewhere.[28] The pigment was purified by solvent extraction (soxhlet) until reaching 98% purity and characterized by ^{1}H and ^{13}C nuclear magnetic resonance spectroscopy, ultraviolet-visible (UV-vis) spectroscopy, mass spectrometry, and infrared spectroscopy.[29] Lipid myristyl myristate (MM, Crodamol® MM, melting point = 36–40 °C) was kindly donated by CRODA® (Argentina). Poloxamer P188 (Kolliphor® P188), and 3,3′-dioctadecyloxacarbocyanine perchlorate ($DiOC_{18}$) were purchased from Sigma-Aldrich.

Synthesis of surface-active ionic liquid (SAIL)

SAILs studied in the present work are displayed in Table 1. The SAIL synthesis was performed following the methodology previously reported and were dried in vacuum prior to use.[21,30–33] Nuclear Magnetic Resonance (NMR) and infrared characterization of all SAILs were carried out using a Bruker Avance 300 NMR spectrometer (Billerica, Ma, USA) and a Bruker Avance 300 NMR spectrometer One Fourier-transform infrared (FTIR) spectrophotometer (Walthan, Ma, USA) respectively.[32]

Synthesis of 1-alkylimidazolium-based surfactants

The synthesis of these SAILs consists of two steps. The first one involves the deprotonation of imidazole followed by nucleophilic displacement with the corresponding 1-bromoalkane to produce the 1-alkylimidazole compounds. The second reaction involves the neutralization of 1-alkylimidazoles using Brønsted acids (molar ratio of base : acid = 1 : 1). In the present work, acetic (CH_3CO_2H), methanesulfonic (CH_3SO_3H) and trifluoracetic (CF_3CO_2H) acids were used as counterions as was previously reported. The acids were slowly added to 1-alkylimidazole dissolved in a minimum amount of anhydrous solvent (acetonitrile and hexane for C_{16}Him) in a two-necked round-bottom flask under stirring at 0 °C. A white solid precipitate formed immediately. The reaction mixture was stirred at the same temperature for an additional period of 2 h.[21] The solvent was evaporated, and the resulting SAILs were exhaustively dried under high vacuum and protected from light for 3 days.

Synthesis of 1-hexadecyl-3-methylimidazolium bromide-based surfactant

This SAIL was prepared from 1-bromohexadecane with 1-methylimidazole conveniently purified. The reactions were performed in toluene under reflux at *ca.* 110 °C in the presence of a 15% excess of 1-bromoalkane for 24 h. The solvent was carefully removed under reduced pressure. The [C_{16}mim]-Br residues obtained were washed with ethyl acetate until bromoalkane had been completely removed. The resulting salts were dried in vacuum for 24–72 h to give white solid powder.

Micellar solution stability

The ability of SAILS to kept Viol in micellar solution was analysed. Aqueous solutions were prepared with 1 mM Viol and 1 mM SAILS concentration, and 5.0 mL final volume. The control was made with Viol dissolved in water. The solutions

Table 1 Depiction of SAILS tested in the present work[a]

Structure	Side chain length (n)	Counterion	Abbreviation
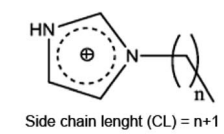 Side chain lenght (CL) = n+1 **[C_nHim]**	9	[CH_3SO_3], S	[C_{10}Him]-S
	11		[C_{12}Him]-S
	13		[C_{14}Him]-S
	15		[C_{16}Him]-S
	9	[CF_3CO_2], F	[C_{10}Him]-F
	11		[C_{12}Him]-F
	13		[C_{14}Him]-F
	15		[C_{16}Him]-F
	15	[CH_3CO_2], Ac	[C_{16}Him]-Ac
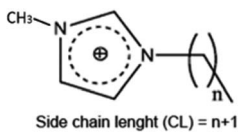 Side chain lenght (CL) = n+1 **[$C_n$mim]**	15	Bromide, Br	[C_{16}mim]-Br

[a] Abbreviation: **[C_nHim]**, 1-alkylimidazole and [C_{16}mim], 1-hexadecyl-3-methylimidazolium.

were filtered through a 0.22 μm syringe cellulose filter and the Viol concentration was determined at $\lambda_{max} = 580$ nm at 0 h, 24 h and 48 h. The data was normalized by A580 maximum which correspond to ([C_{16}Him]-S) at 0 h (with no Viol retained in the filter). Also, solutions of 10 μm Viol with all SAILs were prepared in triplicates and with proper control and absorbance determined at $\lambda_{max} = 580$ nm in order to exclude the effects of micellar polarity being the source of absorbance change instead of changes of Viol concentration associated with SAILs. ANOVA test did not find significant differences between solutions in this control ($p > 0.05$) (Fig. S2†).

SLN preparation

Viol loaded SLNs were prepared by melting 800 mg of MM in a water bath and adding Viol previously dissolved in 200 μL of DMSO (lipid phase). Then, 20.0 mL of an aqueous solution of Poloxamer® P188 (3.0%, w/v), preheated in the same water bath as the lipid (aqueous phase), was poured over the lipid phase. Immediately, the mixture was sonicated in a 130 W at 80% power in ultrasonic processor (Cole-Parmer, USA) for 20 min. Later, the lipid suspension was cooled down to room temperature in a water bath.

In a second formulation (SLN-Viol-SAIL), the surfactant (Poloxamer® P188) was partially replaced with SAIL. In a third one (SLN-Viol-SAIL-FA) folic acid was added to the aqueous phase before the mixing procedure. The chemical composition of different formulations is listed in Table 2.

Encapsulation efficiency

All three formulations were independently prepared in triplicate, and their encapsulation efficiency was measured as follows: immediately after cooling the SLN suspension, the total volume was measured, and 400 μL of it was centrifuged in a Microcon® centrifugal device (10 kDa, Merck Millipore, Billerica, MA, USA).

Viol concentration was measured by absorbance at 580 nm with a proper calibration curve. FA was determined using a calibration curve at 368 nm and 283 nm.

Encapsulation efficiency (EE, %) was calculated as follows:

$$\mathrm{EE}(\%) = \frac{m_0 - (C_{cf} \times V_f)}{m_0} \times 100$$

where m_0 is the initial Viol mass, C_{cf} is Viol concentration in the eluted fraction after centrifugation, and V_f the final volume of suspension after sonication.

Photon correlation spectroscopy

The average hydrodynamic diameter (ζ_{ave}), polydispersity index (PdI), and Z-potential (ζ) were determined by photon correlation spectroscopy with Zetasizer Nano series (Malvern Instruments, U.K.) at 25 °C, after adequate dilution with ultrapure water. All samples were measured in triplicate. Data obtained were analysed by the software provided by Malvern Panalytical.

FTIR analysis

Attenuated total reflectance-FTIR was used to obtain the spectra of all components and formulations in a Spotlight 400-Perkin-Elmer Spectrometer (Waltham, MA, USA). Each spectrum was scanned 32 times and recorded over 550 to 4000 cm^{-1} with a 2 cm^{-1} resolution in triplicate.

XPS analysis

X-ray photoelectron emission analysis was performed on freeze-dried samples in duplicate in an XPS K-Alpha model (Thermo Scientific, USA).

XRD analysis

X-ray diffraction analysis was performed on freeze-dried samples in DRX7000 Shimadzu equipment at Chemical Institute UNICAMP using a copper target, 40 kV, 30 mA, in a range covering from $2\theta = 5°$ to 50° and at a rate of 2° min^{-1}.

Cryo-TEM image acquisition

The samples were prepared in a Lacey Carbon Type 300 mesh copper grid (Ted Pella, USA), and were submitted to the Glow Discharge procedure in easiGlow equipment (Pelco, USA), with the following parameters: current of 15 mA; negative charge; 25 seconds of discharge.

Freezing in amorphous ice (cryo preparation) was done using Vitrobot Mark IV (Thermo Fischer Scientific) equipment at controlled temperature (22 °C) and humidity (100%). Sample preparations were performed with the following parameters: blot time 3 seconds; blot force 0, blot wait 10 seconds with a single blot. Then, 3.0 μL of each sample was applied to the grids and immersed in liquid ethane. After the immersion, the

Table 2 Chemical composition of solid lipid nanoparticle formulations containing violacein[a]

Phase	Lipid phase		Aqueous phase ($V_f = 20$ mL)		
Substance	MM (mg)	Viol (μmol)	P188 (%, w/v)	[C_{16}Im]-S (%, w/v)	FA (mg)
[SLN-Viol]	800	20	3.00	—	—
[SLN-Viol-SAIL]			2.95	0.05	
[SLN-Viol-SAIL-FA]					3.0

[a] Abbreviations: SAIL, [C_{16}Him]-S and FA, folic acid.

grid was maintained in liquid nitrogen until microscopic analysis.

TEM image acquisition

TEM analysis was performed using a Jeol-1200 EX II-TEM microscope (Jeol, Columbia, MD, USA). Nanoparticle dispersions were 1 : 100 diluted with ultrapure Milli-Q® water, and 10 μL of each formulation was spread onto a Cu grid of 400 mesh. After incubation, the sample excess was removed with filter paper. One drop of phosphotungstic acid was added to the grid, for contrast enhancement, and incubated at 25 °C for 1 min before excess removal. Finally, the grid was dried at room temperature.

Cytotoxicity studies

Adenocarcinoma human alveolar basal epithelial A549 cells were cultured in Dulbecco's Modified Eagle's Medium (DMEM; Gibco Invitrogen Corporation, USA) supplemented with 10% fetal bovine serum (Natocor, Córdoba, Argentina) and antibiotics (100 U mL^{-1} penicillin and 0.1 mg mL^{-1} streptomycin from Gibco Invitrogen Corporation, USA) in 5% CO_2 at 37 °C. Cell viability was determined by the MTT [3-(4,5-dimethylthiazol-2-yl)-2,5-diphenyltetrazolium bromide] assay (Mossman, 1983). A549 cells (4.0×10^3 cells per mL) were seeded in 96-well plates and incubated overnight under standard conditions. Thereafter, they were treated with different imidazolic ionic liquids for 48 h. Because of some of the ionic liquids have limited solubility in aqueous media, a minimal volume of DMSO was added reaching a maximum final concentration in the vehicle of 0.05% (v/v).

After treatments, 100 μL of MTT solution (500 μg mL^{-1} MTT in PBS) was added to each well and incubated at 37 °C for 3 h. The resulting formazan crystals were dissolved in 100 μL DMSO, and the absorbance was analysed at 560 nm in a microplate reader (Beckman Coulter DTX 880 Multimode Detector, CA, USA).

SLN cytotoxicity studies

Once SLNs were characterized, their cytotoxicity was studied by the MTT assay, as was described previously for SAILs. In this case, three cell lines were studied: HeLa (human cervical cancer cells), HCT-116 (human colorectal carcinoma cells), and the previously reported A549 cells. Controls for each inactive formulation component (FA, MM, and P188) were performed to discard any toxicity of these substances. Statistical treatment was performed in Sigma Stat software.

Cellular uptake

Cellular uptake was analysed by fluorescence analysis. Briefly, the three formulations were produced as described before, but instead of Viol normal cargo, 0.75 μg mL^{-1} of the green fluorescent dye 3,3′-dioctadecyloxacarbocyanine perchlorate ($DiOC_{18}$, $\lambda_{ex}/\lambda_{em} = 484/501$ nm) was added. HeLa, HCT-116, and A549 cells were seeded at a density of 4.0×10^3 cells per mL in 96-well plates for 24 h. Then, cells were exposed to free MEM containing increasing concentrations of the formulations (0.05 to 0.50 mg lipid matrix per mL) for 24 h. The medium was removed, and cells were washed three times with 200 μL PBS. Finally, fluorescence was determined in a microplate reader (Beckman Coulter DTX 880 Multimode Detector, USA).

Statistical analysis

Analysis of variance (ANOVA) and other statistical analyses were performed in R software.[34]

Results and discussion

Surface-active ionic liquid screening

The first criterion to determine the feasibility of SAILs to be considered for potential development of drug delivery devices is the cytotoxicity. The analysis of SAIL cytotoxicity was performed on human lung carcinoma A549 cells, similarly to previous studies with SAILs.[35,36] SAILS containing different alkyl side chain length from $n = 10$ to 16 synthesized in the present work (*i.e.* ([**C_nHim**]-S) and ([**C_nHim**]-F)) allow for a better understanding of the role of structure–toxicity relationship and the selection of the best candidates for the synthesis of drug delivery formulations for Viol. The cytotoxicity assays of 1.5×10^{-3}% (w/v) (36.9 μM to 49.3 μM) ILs on A549 cells were analysed statistically with two-way ANOVA. For the analysis of the results two factors were considered: the systematic variation of the alkyl chain length in the imidazolic ring (n) and the effect of the counterions. Both factors and the interaction between them have a significant effect on Viol encapsulation ($p < 0.0001$).

The results indicate that the rise of SAIL cytotoxicity in A549 cells can be correlated with the increase of the aliphatic side chain length, as was previously reported.[35] Moreover, different anions can also change the cytotoxicity in A549 cells. However, this effect is not independent of n. In this case, the n effect is stronger on F than on S anion probably because of some interaction between the alkyl side chains within $(CH_3SO_3)^-$ anion (Fig. 1).

On the other hand, F and S anions do not have a significant impact on micellar stability and Viol solubilization ($p > 0.05$). Besides, ([C_{16}Him]-F) and ([C_{16}Him]-S) show no significant differences between them at 24 and 48 h ($p > 0.05$), although they show differences at time zero ($p < 0.01$). Considering these

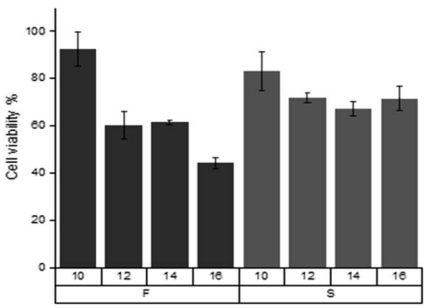

Fig. 1 Viability of A549 cell cultures in presence of [C_nHim]-S and [C_nHim]-F with $n = 10$ to 16.

results, two additional SAILs were tested for cytotoxicity and interaction with Viol, both with $n = 16$. One of them has acetate ($[CH_3CO_2^-]$, Ac) as counterion and the other is of type $[C_{16}mim]$ with bromide (Br^-) as counterion. In these cases, not only a new counterion but also the change of the proton in the imidazole ring by a methyl group were evaluated. Nonetheless, SAIL type $[C_{16}mim]$-Br showed high cytotoxicity at 1.5×10^{-3}% (w/v) and at low concentrations (data not shown), and $[C_{16}Him]$-Ac was found to be insoluble in water. For these reasons, both SAILs were discarded for further studies.

In addition, SAIL interactions with standardized Viol concentrations seem to strongly depend on n length (Fig. 2). However, all the SAILs tested are significantly different from the control. SAILs containing longer side chains can bring more Viol into solution, and the resulting micelles can sustain Viol for longer periods of time ($p < 0.0001$). This effect could be associated with the hydrophobic nature of the alkane side chain length, which increases with n and enhances the interaction SAIL-Viol, interfering with the Viol–Viol contact mediated by the hydroxyindole rings.

Based on the present results, the best candidate to develop a Viol drug delivery system was $[C_{16}Him]$-S, which combines low cytotoxicity with 71.5% cell viability at 1.5×10^{-3}% (w/v) and good interaction with 95.2% of Viol retained in micellar solution for at least 48 h.

Viol-IL FTIR

The FTIR spectra corresponding to $[C_{16}Him]$-S, Viol and the system formed by equimolecular amount both components (SAIL-Viol) are shown in Fig. 3. The $[C_{16}Him]$-S spectrum, the bands corresponding to 633.6 cm^{-1}, 766.4 cm^{-1} and 901.7 cm^{-1} were attributed to deformation out of plane, C–H out of plane and ring deformation in plane of imidazolic ring, respectively (Fig. 3A). Peaks at 1091.2 cm^{-1}, 1549.1 cm^{-1}, 1582.3 cm^{-1} were attributed to C–N and C=N stretching vibrations. Alkyl group of $[C_{16}Him]$ displayed at 1465.0 cm^{-1} peak corresponds to C–H bending, 2849.8 cm^{-1} to $-CH_2$ symmetric stretching and 2919.8 cm^{-1} to $-CH_2$ asymmetric stretching. On the other side sharp bands at 1034.5 cm^{-1} and 1230.6 cm^{-1} were attributed to the S=O and S–O stretching vibrations on IL counterion. Finally, wide band at 3432.3 cm^{-1} was assigned to N–H stretching vibration similarly as previously reported.[37–41]

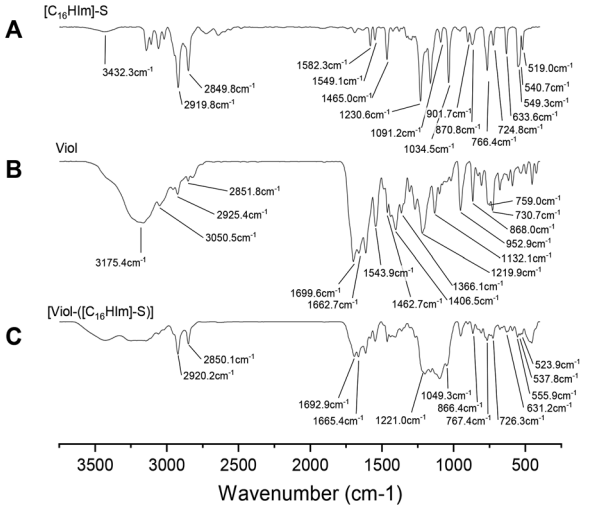

Fig. 3 FTIR spectra of $[C_{16}Him]$-S (A), Viol (B) and [Viol-($[C_{16}Him]$-S)] (C).

The Viol spectrum showed large wide peak at 3175.4 cm^{-1} attributed to some moisture remained in the sample overlapping the weak OH stretching band in the same region (Fig. 3B). Partially overlapped bands at 730.7 cm^{-1} and 759 cm^{-1} were attributed to C–H stretching and bending in monosubstituted benzene. The bands at 868.0 cm^{-1}, 952.9 cm^{-1}, 1132.1 cm^{-1} and 1219.9 cm^{-1} were assigned to different C–N symmetric and asymmetric stretching vibrations and band at 1366.1 cm^{-1} N–H overlapped with C–O stretching, band at 1406.5 cm^{-1} C–H bending on alkene, 1462.7 cm^{-1}, 1543.9 cm^{-1} and 1662.7 cm^{-1} bands C=C stretching in aromatic benzene and strong band at 1699.6 cm^{-1} carbonyl stretching vibrations. Complex and wide peak at higher frequencies comprises different and highly overlapped N–H and O–H stretching frequencies (2851.8 cm^{-1}, 2925.4 cm^{-1}, 3050.5 cm^{-1} and 3175.4 cm^{-1}).[2,42,43]

Several shifts were observed in equimolar mixture [Viol-(C_{16}Him-S)] and a complex spectrum was observed (Fig. 3C). At low frequencies range (500–670 cm^{-1}) intensities are low and displayed many peaks as previously reported.[43] This region displayed intramolecular vibrational modes of the skeletal vibration of the imidazolium ring, two peaks in this region showed a hypsochromic shifts from 549.3 cm^{-1} to 555.9 cm^{-1}, and 519 cm^{-1} to 523.9 cm^{-1}, and two bathochromic shifts from 540.7 cm^{-1} to 537.8 cm^{-1} and 633.6 cm^{-1} in pure IL to 631.2 cm^{-1} in the complex. In the 700–900 cm^{-1} region peaks corresponding to C–H bending in rings described before in both $[C_{16}Him]$ and Viol fused peaks are observed, 724.8 cm^{-1} peak in $[C_{16}Him]$ and 730.7 cm^{-1} peak in Viol appear as one peak at 726.3 cm^{-1}, in a similar way, 766.4 cm^{-1} peak in

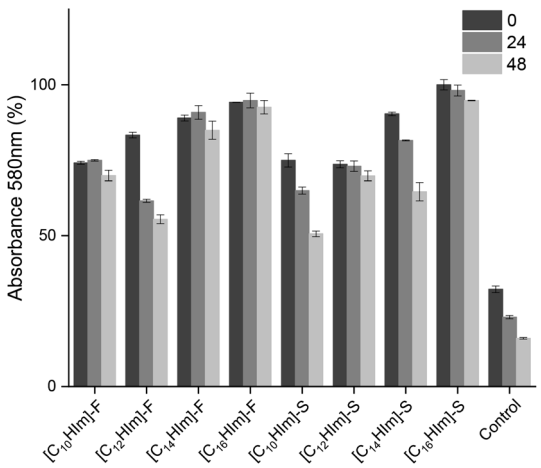

Fig. 2 Effect of the length of alkyl side carbon chains and anions on the stability of micellar solutions of [Viol-($[C_nHim]$-S)] and [Viol-($[C_nHim]$-F)] at 0, 24 and 48 h.

[C_{16}Him] and 759.0 cm^{-1} in Viol appear as one peak at 767.4 cm^{-1} in the mixture, and 870.8 cm^{-1} and 868.0 cm^{-1} appear as one peak at 866.4 cm^{-1}. Among others, carbonyl bands at 1662.7 cm^{-1} and 1699.6 cm^{-1} in pure Viol were switched to 1665.4 cm^{-1} and 1692.9 cm^{-1}, respectively.

Finally, the peaks corresponding to sulfonate group counterion of SAIL (1034.5 cm^{-1} and 1230.6 cm^{-1}) do not appear strongly in the mixture and the peaks closest to those that can be assigned in the mixture are 1049.3 cm^{-1} and a shoulder at 1221.0 cm^{-1} respectively. No relevant shifts are observed in bands related to alkylic chains (2850.1 cm^{-1} and 2920.2 cm^{-1}).

All this data taken together suggest a π–π stacking strong interaction between Viol and [C_{16}Him]-S centred on and between aromatic rings, and displacement of the $(CH_3SO_3)^-$ counterion.

SLN analysis

Considering the low stability of micellar systems, which is environmentally dependent (*i.e.* pH, T, I, *etc.*), a stable drug carrier for SAILs needs to be developed. Since [C_{16}Him]-S was selected as primary carrier for Viol, SLN appears a feasible alternative. Also, the resulting SLNs tailored with folate allow cancer cell targeting. In the final SLN formulations, drug/carrier ratio was 0.49 mg Viol/100 mg carrier; and drug/lipid ratio was 0.86 mg Viol/100 mg lipid.

Encapsulation efficiency increased significantly by approximately 8.0% ($p < 0.05$) after the inclusion of [C_{16}Him]-S in SLN formulation. This can be explained by the intrinsic affinity between Viol and SAIL described previously. However, all three formulations possess a very high EE%, explained by the poor solubility of Viol in aqueous solutions (Table 3).

Physicochemical characterization

Photon correlation spectroscopy. The ζ_{ave}, PdI, and ζ for each formulation are shown in Table 4. Every measurement reached the quality criteria suggested by the software. [C_{16}Him]-S addition to the aqueous phase significantly decreases the particle hydrodynamic radius (RH) ($p < 0.0001$) from 203.1 nm in SLN-Viol to 173.8 nm in [SLN-Viol-([C_{16}Im]-S)], but it does not change the PdI ($p > 0.05$). However, a mayor change is observed in ζ as is expected. P188 is a non-ionic surfactant, which explains the near-zero ζ observed in SLN-Viol; the addition of a cationic SAIL such as [C_{16}Him]-S greatly increases ζ in SLN-Viol-SAIL ($p < 0.0001$) indicating that SAIL is on the particle surface.

Table 3 Encapsulation efficiency of violacein in solid lipid nanoparticles in presence of [C_{16}Him]-S and folic acid (FA)

Formulation	Violacein encapsulation (%)
[SLN-Viol]	91.0 ± 1.0
[SLN-Viol-([C_{16} Him]-S)]	99.2 ± 0.5
[SLN-Viol-([C_{16}Him]-S)-FA]	98.2 ± 0.6

Table 4 Properties of different solid lipid nanoparticles containing violacein analysed by DLS

Formulation	Size (R_H) (nm)	PdI	ζ (mV)
[SLN-Viol]	203.1	0.224	−2.9
[SLN-Viol-([C_{16}Him]-S)]	173.8	0.241	39.9
[SLN-Viol-([C_{16}Him]-S)-FA]	199.0	0.387	41.5

FA in [SLN-Viol-SAIL]-FA does not seem to significantly modify ζ from SLN-Viol-SAIL, but it does increase PdI from other formulations. The cause of this increase is a second intensity peak a very high size (5039 nm) in the size distribution plot, probably due to some particle aggregation that may have occurred between the preparation and the measurement (data not shown).

XPS analysis

Surface analysis by XPS results are displayed in Table 5. SLN-Viol does not show nitrogen, indicating that there is no Viol on the particle surface; C and O are attributable to P188 surfactant and myristyl myristate. SLN-Viol-SAIL shows nitrogen and sulphur, indicating that [C_{16}Him]-S is on the particle surface, in concordance with DLS data. [SLN-Viol-([C_{16}Him]-S)]-FA shows a decrease in sulphur percentage, which can be a displacement of methanesulfonate covered by folate.

FTIR analysis

All three SLN formulations showed the characteristic peaks of MM, 719 cm^{-1} for $-CH_2$ rocking, 1463 cm^{-1} and 1473 cm^{-1} for $-CH_2$ scissoring, 1734 cm^{-1} for stretching vibration of ester group, 2849 cm^{-1} for $-CH_2$ symmetric stretching, and 2917 cm^{-1} for the asymmetric stretching of $-CH_2$ (Fig. 4).[44]

In addition, the SLN-Viol formulation containing P188 showed a broad peak at 3448 cm^{-1} attributed to vibrations coming from hydroxyl groups. The peak at 952 cm^{-1}, which could be attributed to C–O symmetric stretching for SLN-Viol, displayed a blue shift to 954 cm^{-1} and 956 cm^{-1} for [SLN-Viol-([C_{16}Him]-S)] and [SLN-Viol-([C_{16}Him]-S)]-FA respectively.

Also, the asymmetric stretching of ether groups at 1102 cm^{-1} for SLN-Viol displayed a blue shift at 1104 cm^{-1} for [SLN-Viol-([C_{16}Him]-S)] and at 1106 cm^{-1} for [SLN-Viol-([C_{16}Him]-S)]-FA respectively. This last shift can be explained by the intrusion of P188 and [C_{16}Him]-S first and FA later into [SLN-Viol-([C_{16}Him]-S)] and [SLN-Viol-([C_{16}Him]-S)]-FA respectively (Fig. 4).

XRD analysis

The diffraction patterns of all three formulations showed peaks at 8.02°, 19.43°, 22.01°, and partially overlapped peaks at 23.60° and 24.12°. Peaks at 8.02°, 22.01°, and 24.12° also appear on MM diffraction patterns, as well as peaks at 19.43° and 23.60° on P188 diffraction patterns. However, there are no significant differences between formulations and no peaks from other components. All these data suggest molecularly dispersed Viol,

Table 5 XPS analysis of different solid lipid nanoparticles containing violacein

Formulation	Composition (%)			
	C 1s	O 1s	N 1s	S 2p
[SLN-Viol]	83.7 ± 0.5	16.4 ± 0.5	—	—
[SLN-Viol-([C_{16}Him]-S)]	85.5 ± 0.2	13.0 ± 0.7	0.6 ± 0.1	0.4 ± 0.1
[SLN-Viol-([C_{16} Him]-S)-FA]	84.9 ± 1.2	14.7 ± 0.6	0.6 ± 0.1	0.3 ± 0.1

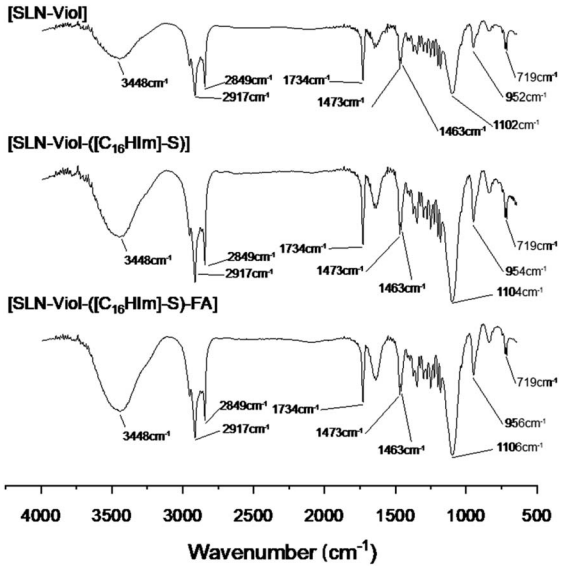

Fig. 4 FTIR spectra of different SLN formulations containing violacein.

while MM and P188 crystallinity inside the particles remains, as was reported previously.[44]

Microscopy images

Cryo-TEM and TEM image analysis. Cryo-TEM images showed that NLCs were spheroidal with 155 nm in average diameter (SD = 14, n = 14) for SLN-Viol, an average 155 nm (SD = 68, n = 11) for [SLN-Viol-([C_{16}Him]-S)], and an average 168 nm (SD = 60, n = 9) for [SLN-Viol-([C_{16}Him]-S)]-FA. Moreover, [SLN-Viol-([C_{16}Him]-S)]-FA showed dot-like structures absent in previous formulations, which can be attributed to the presence of folate in the SLN (Fig. 5).

TEM images were recorded to confirm Cryo-TEM observations. TEM displays high image contrast that allowed a better identification of the structures in SLN-Viol, which are approximately round with sizes in the range of 100 nm to 200 nm, and around 160 nm in [SLN-Viol-([C_{16}Him]-S)] (Fig. 6).

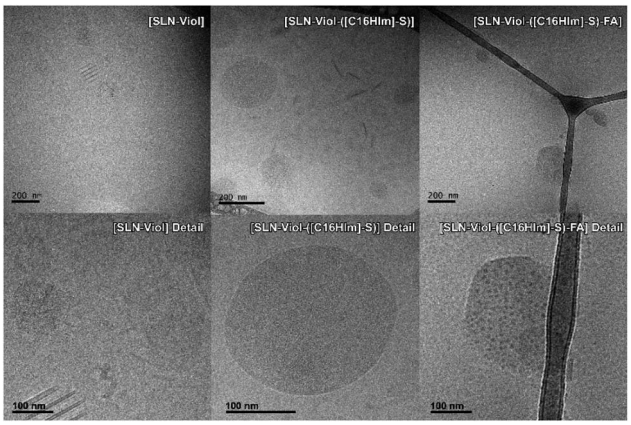

Fig. 5 Cryo-TEM images of different violacein formulations.

In vitro toxicity studies

The cytotoxic activity of the different lipid formulations was evaluated on A549, HCT-116, and HeLa cells exposed to increased amounts of free or encapsulated Viol (0.0–4.0 μM) for 24 h, according to previous publication.[14] Cytotoxic effects are considered when a growth cell reduction is higher than 30% in cell viability following ISO 10993-52,009 standard. Firstly, we analysed the effect of the free-violacein nanoparticles on the three cell lines. Cells were exposed to 0.04 and 0.16 mg mL^{-1} MM [SLN-([C_{16}Him]-S)] (equivalent to those necessary to deliver Viol 1.0 and 4.0 μM) for 24 h. It was found that 0.04 mg mL^{-1} [SLN-Viol-([C_{16}Him]-S)] induced a cell growth inhibition of 5.5, 21.8 and 20.0% whereas 0.16 mg mL^{-1} promoted an inhibition of 9.9, 24.0, and 24.8% in A549, HCT-116 and Hela cells, respectively (Fig. S3†). These results evidence that empty [SLN-Viol-([C_{16}Him]-S)] are not toxic in our culture conditions. HeLa cells were more sensitive to Viol than A549 and HCT-116 cells since free Viol was cytotoxic from 0.25 μM in HeLa cells and from 2.0 μM in A549 and HCT-116 (Fig. 7).

The calculated IC_{50} values for the tested formulations are listed in Table 6.

Viol encapsulation into the three different systems, [SLN-Viol], [SLN-Viol-([C_{16}Him]-S)] and [SLN-Viol-([C_{16}Him]-S)-FA], improved its cytotoxicity at lower concentrations in A549 and HCT-116 cells, particularly in colorectal carcinoma cells, suggesting that SLN encapsulation potentiates the anticancer activity of Viol at low concentrations in these cell lines.

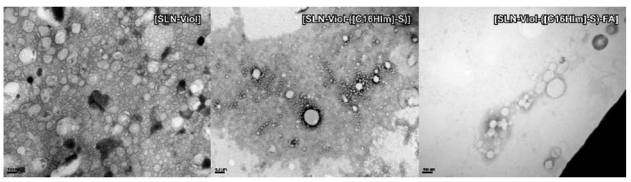

Fig. 6 TEM images of different violacein formulations.

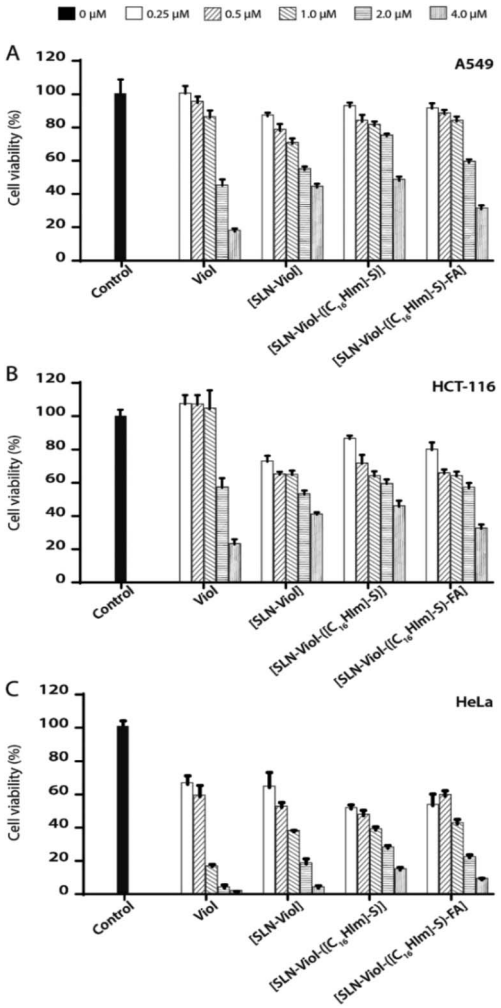

Fig. 7 Cell viability of A549 (A), HCT-116 (B) and HeLa (C) in presence 0.25 μM, 0.5 μM, 1.0 μM, 2.0 μM and 4.0 μM of violacein and violacein formulations.

However, from 2.0 μM, free Viol was more cytotoxic than the encapsulated Viol in the three cell lines tested.

This phenomenon was previously observed in HCT-116 cells exposed to emulsified Viol and may reflect the fact that SLN-encapsulated Viol is released in a time-dependent controlled manner. Besides, the main concern related to emulsified formulations is the instability strongly mediated by shelf time and environmental conditions.[14]

Table 6 Inhibitory effect (IC_{50}) of violacein and different solid lipid nanoparticle formulations containing violacein on HeLa, HCT-116 and A549 cell lines incubated for 24 h

	Cell lines		
IC_{50} (μM)	HeLa	HCT-116	A549
Viol	0.71	1.51	1.30
[SLN-Viol]	0.75	1.44	1.66
[SLN-Viol-([C_{16}Him]-S)]	0.63	1.64	2.23
[SLN-Viol-([C_{16}Him]-S)-FA]	0.74	1.33	1.51

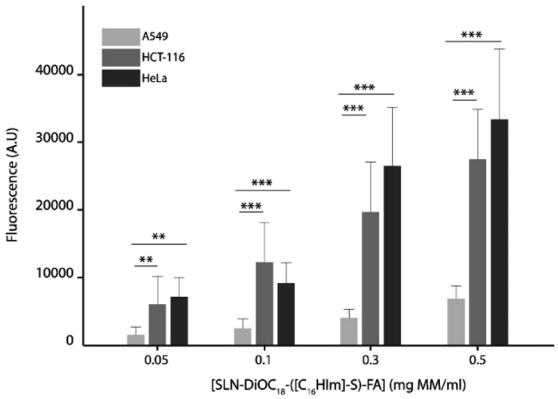

Fig. 8 Effect of [SLN-$DiOC_{18}$-([C_{16}Him]-S)-FA] concentrations on the cellular uptake by A549, HCT-116 and HeLa cells.

When IC_{50} values for Viol-loaded nanoparticles were compared, data showed no significant differences between formulations, except for [SLN-Viol], [SLN-Viol-([C_{16}Him]-S)] on A549 cells, in which IC_{50} value was significantly higher (Table 6). As observed for free Viol, HeLa proved to be the most sensitive cell line to Viol loaded nanoparticles.

Cellular uptake

The efficient incorporation of the nanoparticles into the cells and the targeting activity of folate-decorated surface nanoparticles were assessed. For that purpose, cancer cell lines that do to not express the folate receptor such as A549 cell lines or overexpress the folate receptor such as HCT-116 and HeLa were tested.[45,46] A dose-dependent incorporation of the fluorescent labelled nanoparticles into the three cell lines was observed (Fig. 8).

However, the incorporation of the nanoparticle into the cells was mediated by the presence of the folate receptor in the different cell lines, which was up to fivefold higher in cells overexpressing the folate receptor than cells that do not express it.

Conclusions

ILs with surfactant derivatives of 1-alkylimidazolium cations and different counterions were tested for their ability to interact with Viol and remain in solution, as well as for their toxicities to A549 cell line. The results indicate an enhanced cytotoxicity when a hydrogen linked to the nitrogen (3-N) of the imidazole ring is replaced by a methyl group ([C_{16}mim]-Br).

In addition, the present work demonstrated that SAIL counterions play a major role in micellar stability and in cytotoxicity. The synthesis of SAILs with a delicate equilibrium of hydrophilic–hydrophobic components will allow the dissolution of poor water-soluble molecules such as violacein without compromising cell cytotoxicity. The conjunction of imidazole alkyl side chain and counterion in the SAILs tested resulted in the selection of [C_{16}Him]-S to develop a micellar solution of Viol. However, the instability of the micellar structure of [Viol-

([C_{16}Him]-S)] required the development of a new type of formulation to be potentially used for therapeutic purposes.

Solid lipid nanoparticles were a good carrier choice for Viol since it is naturally released from bacteria producers *via* membrane vesicles and has high stability and defined controlled release kinetics. Also, NLCs are very versatile drug delivery devices since the chemical composition of the carriers can be adapted to transport molecules with diverse biophysical properties and can be tailored to specific cells with the proper receptors. These results suggest that [SLN-Viol-([C_{16}Him]-S)-FA] formulation is a novel, promising and effective system for targeted delivery of Viol against cancer cells overexpressing the folate receptor.

Conflicts of interest

There are no conflicts to declare.

Acknowledgements

The present work was supported by Universidad Nacional de La Plata (Grants X701) and Agencia Nacional de Promoción Científica y Técnica (ANPCyT, PICT2016-4597) of Argentina to GRC. We want to thank the personnel of the Chemical Institute (UNICAMP) and the National Laboratory of Nanotechnology (LNNano), located at the National Center for Research in Energy and Materials (CNPEM, Campinas, Brazil) for the FTIR and XPS spectra, respectively.

References

1 S. Y. Choi, S. Lim, G. Cho, J. Kwon, W. Mun, H. Im and R. J. Mitchell, *Environ. Microbiol.*, 2020, **22**, 705.
2 C. A. Aruldass, S. Raj, L. Masalamany, C. K. Venil and W. A. Ahmad, *Environ. Sci. Pollut. Res.*, 2018, **25**, 5164.
3 A. C. G. Cauz, G. P. B. Carretero, G. K. V. Saraiva, P. Park, L. Mortara, I. M. Cuccovia, M. Brocchi and F. J. Gueiros-Filho, *ACS Infect. Dis.*, 2019, **5**, 539.
4 E. Bilsland, T. A. Tavella, R. Krogh, J. E. Stokes, A. Roberts, J. Ajioka, D. R. Spring, A. D. Andricopulo, F. T. M. Costa and S. G. Oliver, *BMC Biotechnol.*, 2018, **18**, 22.
5 P. Antonisamy and S. Ignacimuthu, *Phytomedicine*, 2010, **17**, 300.
6 N. Durán, G. Z. Justo, M. Duran, M. Brocchi, L. Cordi, L. Tasic, G. R. Castro and G. Nakazato, *Biotechnol. Adv.*, 2016, **34**, 1030.
7 F. A. Venegas, G. Köllisch, K. Mark, W. E. Diederich, A. Kaufmann, S. Bauer, M. Chavarría, J. J. Araya and A. J. García-Piñeres, *Sci. Rep.*, 2019, **9**, 13661.
8 F. Bray, J. Ferlay, I. Soerjomataram, R. Siegel, L. A. Torre and A. Jemal, *Ca-Cancer J. Clin.*, 2018, **68**, 394.
9 C. V. Ferreira, C. L. Bos, H. H. Versteeg, G. Z. Justo, N. Durán and M. P. Peppelenbosch, *Blood*, 2004, **104**, 1459.
10 D. Platt, S. Amara, T. Mehta, K. Vercuyssee, E. L. Myles, T. Johnson and V. Tiriveedhi, *Biochem. Biophys. Res. Commun.*, 2014, **455**, 107.
11 T. Mehta, K. Vercruysse, T. Johnson, A. O. Ejiofor, E. Myles and Q. A. Quick, *Mol. Med. Rep.*, 2015, **12**, 1443.
12 D. D. de Carvalho, F. T. M. Costa, N. Duran and M. Haun, *Toxicol. in Vitro*, 2006, **20**, 1514.
13 S. M. HasImi, T. Xu and M. Q. Wei, *Oncol. Rep.*, 2015, **33**, 1731.
14 I. Rivero Berti, B. Rodenak-Kladniew, A. A. Perez, L. Santiago, N. Duran and G. R. Castro, *React. Funct. Polym.*, 2019, **136**, 122.
15 K. C. S. Queiroz, R. Milani, R. R. Ruela-de-Sousa, G. M. Fuhler, G. Z. Justo, W. F. Zambuzzi, N. Duran, S. H. Diks, C. S. Spek, C. V. Ferreira and M. P. Peppelenbosch, *PLoS One*, 2012, **7**(10), e45362.
16 N. Bromberg, J. L. Dreyfuss, C. V. Regatieri, M. V. Palladino, N. Durán, H. B. Nader, M. Haun and G. Z. Justo, *Chem.-Biol. Interact.*, 2010, **186**, 43.
17 U. Samanta, D. Pal and P. Chakrabarti, *Acta Crystallogr., Sect. D: Biol. Crystallogr.*, 1999, **55**, 1421.
18 R. Chelli, F. L. Gervasio, P. Procacci and V. Schettino, *J. Am. Chem. Soc.*, 2002, **124**, 6133.
19 C. P. Fredlake, J. M. Crosthwaite, D. G. Hert, S. N. V. K. Aki and J. F. Brennecke, *J. Chem. Eng. Data*, 2004, **49**, 954.
20 J. Claus, F. O. Sommer and U. Kragl, *Solid State Ionics*, 2018, **314**, 119.
21 C. G. Adam and G. G. Fortunato, *J. Surfactants Deterg.*, 2019, **22**, 501.
22 N. Adawiyah, M. Moniruzzaman, S. Hawatulaila and M. Goto, *MedChemComm*, 2016, **7**, 1881.
23 S. Kalepu and V. K. Nekkanti, *Acta Pharm. Sin. B*, 2015, **5**, 442.
24 J. L. Shamshina, P. S. Barber and R. D. Roger, *Expert Opin. Drug Delivery*, 2013, **10**, 1367.
25 G. A. Islan, M. L. Cacicedo, B. Rodenak-Kladniew, N. Durán and G. R. Castro, *Curr. Pharm. Des.*, 2017, **23**, 6643.
26 H. Yoo and T. Park, *J. Controlled Release*, 2004, **100**, 247.
27 S. A. Kularatne and P. S. Low, *Methods Mol. Biol.*, 2010, **624**, 249.
28 A. S. Mendes, J. E. de Carvalho, M. C. T. Duarte, N. Durán and R. E. Bruns, *Biotechnol. Lett.*, 2001, **23**, 1963.
29 D. Rettori and N. Durán, *World J. Microbiol. Biotechnol.*, 1998, **14**, 685.
30 C. G. Adam, M. V. Bravo, P. M. E. Mancini and G. G. Fortunato, *J. Phys. Org. Chem.*, 2014, **27**, 841.
31 T. Mukai, M. Yoshio, T. Kato, M. Yoshizawa and H. Ohno, *Chem. Commun.*, 2005, 1333.
32 R. Vanyúr, L. Biczók and Z. Miskolczy, *Colloids Surf., A*, 2007, **299**, 256.
33 S. J. L. P. Perez and S. D. Arco, *J. Chin. Chem. Soc.*, 2014, **61**, 935.
34 Anonymous. R Core Team, *R: a language and environment for statistical computing*, Vienna, Austria, 2018, https://www.r-project.org/.
35 H. L. Chen, H. F. Kao, J. Y. Wang and G. T. Wei, *J. Chin. Chem. Soc.*, 2014, **61**, 763.
36 N. Madria, T. A. Arunkumar, N. G. Nair, A. Vadapalli, Y. W. Huang, S. C. Jones and V. Prakash Reddy, *J. Power Sources*, 2013, **234**, 277.

37 W. Q. Feng, Y. H. Lu, Y. Chen, Y. W. Lu and T. Yang, *J. Therm. Anal. Calorim.*, 2016, **125**, 143.
38 D. Lin-Vien, N. B. Colthup, W. G. Fateley and J. G. Grasselli, *The handbook of infrared and Raman characteristic frequencies of organic molecules*, Elsevier Science, 1991.
39 R. Ramasamy, *Arm. J. Phys.*, 2015, **8**, 51.
40 L. Zanchet, L. Guerreiro da Trindade, D. W. Lima, W. Bariviera, F. Trombetta, M. Oberson de Souza and E. M. Agostini Martini, *Ionics*, 2019, **25**, 1167.
41 F. A. Fakhr, A. Khanafari, M. Baserisalehi, R. Yaghoobi and S. Shahghasempour, *Afr. J. Microbiol. Res.*, 2012, **6**, 6235.
42 S. Narayanan, T. Prasad and I. C. Nair, *Novus Int. J. Biotechnol. Biosci.*, 2012, **1**, 1.
43 T. Yamada, Y. Tominari, S. Tanaka and M. Mizuno, *J. Phys. Chem. B*, 2017, **121**, 3121.
44 G. A. Islan, P. Cortez Tornello, G. A. Abraham, N. Duran and G. R. Castro, *Colloids Surf., B*, 2016, **143**, 168.
45 Z. Zhang, J. Jia, Y. Lai, Y. Ma, J. Weng and L. Sun, *Bioorg. Med. Chem.*, 2010, **18**, 5528.
46 K. M. Elamin, K. Motoyama, T. Higashi, Y. Yamashita, A. Tokuda and H. Arima, *Int. J. Biol. Macromol.*, 2018, **113**, 386.

